Computerized generation of realistic pulmonary nodule phantoms in helical CT images

Xiangwei Zhang[1], Eric Olcott[2], Philippe Raffy[1], Naichang Yu[1], Haili Chui[1]

[1] Hologic/R2, Santa Clara, CA, 95054 USA
[2] Stanford School of Medicine, Palo Alto, CA, 94087 USA

Abstract. We develop a framework of computerized generating solid pulmonary nodules in real chest helical computed tomography (CT) images. Spheres with random deformations are used to model nodule shapes. The nodule density is represented by a uniform signal with additive zero mean Gaussian noise. The insertion of synthetic nodules into real CT images is formulated as α blending between foreground nodules and background pulmonary tissues. The blending factors reflect not only the partial volume effect but also the smoothing effect in the filtered back projection (FBP) CT reconstruction. A new lesion insertion scheme based on dual source blending is proposed to blend the image noise and the lesion object separately for a better noise model. A subjective evaluation is performed by a human expert; and statistics of simulated nodules and real nodules are compared to give a quantitative analysis. These validations demonstrate a high level of similarity between the synthetic nodules and real nodules. An evaluation study of a commercial Computer-aided detection (CAD) system on an objective database created using this framework is also presented.

1 Introduction

Computer-aided detection (CAD) is a promising tool to assist in lung nodule detection, and to assess lesion size change over time based on computed tomography (CT) scans. The use of CAD may improve the performance of radiologists in helical CT lung screening. Many techniques for automated nodule detection and characterization have been developed [1], [2], [3], [4], [5], [6], [7].

Evaluating these methods is difficult due to the lack of database with large number of nodules/gold standards. Building real nodule database with expert opinions as gold standard [8] suffers from several drawbacks, especially inaccurate volume definition. Physical nodule phantoms can give accurate volume definition, but it is difficult to create large amount of nodules with different characteristics.

Compared to building real nodule CT database and making physical phantoms, computerized generation of synthetic lesions with known characteristics offers a powerful tool for CAD evaluation. A computerized nodule generation method was reported by Raffy et al, where the nodules were modelled as ellipsoids, and the insertion was a direct replacement followed by a smoothing [9]. In our previous work [10], we simulated nodules using deformed spheres, and

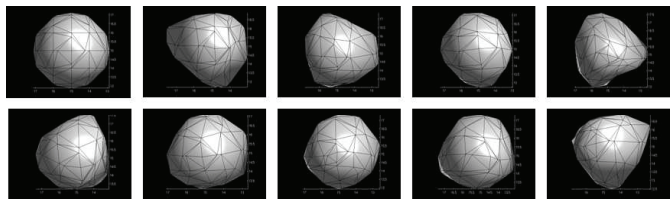

Fig. 1. various nodule shapes created using TPS deformations.

inserted the synthetic nodules into real CT images using 'weighted averaging' between nodules and the background images. Multiple sclerosis lesion phantoms in the magnetic resonance (MR) images were created by Rexilius et al: three different shapes were created to model lesions, each lesion was inserted into MR images using a 'linear combination' of the lesion and the MR scans [11].

In this work, we develop a framework for simulating solid nodules in helical CT images. The simulation method is detailed in Sect. 2, the model validation is described in Sect. 3, an application for CAD evaluation is presented in Sect. 4, and the results are given in Sect. 5.

2 Materials and Methods

A typical pulmonary nodule is about $2mm$ to $30mm$, takes a sphere-like shape. The density of the major core part is similar to muscle and vessel; near the nodule border, the density attenuates gradually until merging into the background. We concentrate on modeling the following characteristics of pulmonary nodules: 1) shape; 2) size; 3) core density; 4) density attenuation on the border.

2.1 Nodule shape/size modeling

Nodule shapes are modeled using unit spheres with randomly generated high dimensional deformations. We adopt the thin-plate spline (TPS) [12] as the non-rigid mapping to do the deformations. TPS deformations can be expressed as:

$$T^{'} = T \cdot d + k \cdot c \tag{1}$$

Here the T is $n \times 4$ matrix in which each row is homogeneous coordinate representation of an original control point. d is 4×4 affine transform matrix. k is a $n \times n$ matrix depending on control points. c is $n \times 4$ matrix in which the first column elements are all zeros, and the remaining three columns consist of randomly distributed deformation coefficients.

Experiments showed that this model is able to generate highly realistic nodule shapes, by tuning the random distribution parameters. In this work, normal

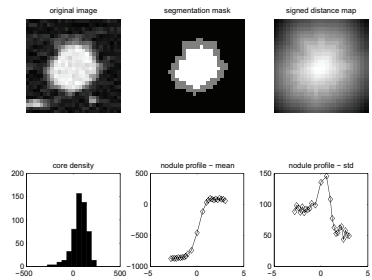

Fig. 2. Nodule density analysis. First row: original image; segmented nodule; signed distance. Second row: histogram of core density; density mean of different layer (indicated by distance values); density variance of different layer.

distribution is used to create deformation coefficients in c. Some examples of synthetic nodule shapes created are illustrated in Fig. 1.

The deformed unit sphere can be easily scaled, rotated, skewed by applying further affine transform by introducing d.

2.2 Nodule density modeling

Density distribution is analyzed for selected real solid nodules with varying sizes, shapes, CT protocols. Only isolated nodules are used, as the non-isolated nodules are difficult to segment, thus, affect the estimation. 100 real nodules from 18 CT exams (0.6-1.3mm collimations, 20-120mAs exposure) are selected.

It is important to distinguish the nodule core part and the volume average layer (due to partial volume effect, reconstruction smoothing effect). Each nodule is analyzed layer by layer from background to the center using a 3D distance transform [13], with the border as feature points, see Fig. 2. The exterior part is set to negative. For each pixel, the distance value indicates the layer – how far it is from the nodule border, and in which direction – toward or away. Note that the variance estimated for the background and volume average layer in Fig. 2 is not valid, due to the structure noise in the background, and the fast changing density in the transition layer.

It has been showed that the density of each individual core follows an approximate Gaussian distribution, but the means and variances vary across nodules and cases. For filtered back projection (FBP), the noise variance in CT images is a slowly varying spatial function [14]. In this work, stochastic noise for each simulated nodule is represented by additive Gaussian noise, and the noise variance is estimated from a neighboring structure in real CT images with water-like attenuation, either nearby vessels or chest walls. We represent the density of nodule core as $I_o = \bar{I}_o + N_o(0, \sigma_o)$, with I_o being the nodule density, $\bar{I}_o$ being

object density, N_o being the zero mean Gaussian noise. For volume average layers, there is a gradual density reduction from interior layers to exterior layers. The thickness of volume average layers is related to reconstruction kernels, and is also estimated. The modeling of volume average layer is described later.

2.3 Nodule insertion using dual source α blending

In this work, inserting synthetic lesions into real images is newly formulated as α blending, a common technique in computer graphics [15]. Given source and destination images, we can control blending on a pixel by pixel basis. Specifically, each pixel of the synthetic nodule is the source with blending factor α, and pixel of the CT scan at corresponding location is the destination with a blending factor $1 - \alpha$. Note that the blending factor is a function of pixel positions.

The first step is the rasterization of the continuous nodule shape in digital space with higher resolution (for better accuracy) than the original scan. The cuboid region of interest (ROI) need to include both the core and the volume averaging layer. This step leads to a binary representation of the synthetic shape with 1 for interior, and 0 for exterior. The volume of the nodule is the total number of the interior pixels multiplied by the volume of each pixel.

The second step is to calculate the α. We simulate the partial volume effect using α channel antialiasing. α value for a pixel is set to be a number between 0 and 1 that is the percentage of that pixel covered by the nodule. A pixel in ROI with the original resolution corresponds to a larger cuboid in the high resolution binary image, and the α value should be the percentage of that cuboid covered by the nodule – this is implemented by rasterization of the cuboid in the high resolution space, trilinear interpolation in the binary image, and averaging over the cuboid. This results in volume average layer with a single pixel thickness. The volume average layer can be more than a single pixel layer, depending on the reconstruction kernel used in FBP. To simulate this smoothing effect, we add a Gaussian smoothing on the binary image, so that interpolation occurs on a smoothed gray scale image. The kernel size is chosen roughly as the thickness of the transition layer.

The third step is to do the blending. Given the α value for each pixel of the ROI in the original CT image resolution, the blending can be described as

$$I = \alpha I_o + (1 - \alpha) I_b \tag{2}$$

where I is the final density, I_o the nodule density, I_b the background density. Similar technique were reported [10], [11], but not formulated as α blending. This single source α blending gives us a better solution than direct smoothing [9], but the volume average layer is still visually artificial – obviously less noisy than both the nodule core part, and the background. The explanation comes from the following analysis.

Similar to the representation of nodule density as $I_o = \bar{I}_o + N_o(0, \sigma_o)$; we can also describe the background as $I_b = \bar{I}_b + N_b(0, \sigma_b)$, with I_b the background density, $\bar{I}_b$ the background density without noise, N_b the zero mean Gaussian

noise. (Note that this formula is just for convenience of analysis, it does not mean we can explicitly separate the true signal and the noise for the background. The reason we can model a solid nodule explicitly using a constant density with additive Gaussian noise is that we can reasonably assume that a solid nodule has a similar density at the major core; this assumption obviously does not hold for complicated lung field.) Then formula (2) becomes

$$I = \bar{I} + n; \quad with \quad \bar{I} = \alpha \bar{I}_o + (1-\alpha)\bar{I}_b, \quad n = \alpha N_o + (1-\alpha)N_b \tag{3}$$

with $\bar{I}$ being the blending results without noise, and n is the combined noise after the blending. The mean and the variance of the combined noise are

$$E(n) = 0; \quad \sigma_n^2 = \alpha^2\sigma_o^2 + (1-\alpha)^2\sigma_b^2 \tag{4}$$

By assuming $\sigma_o = \sigma_b = \sigma$ (due to the slow changing of noise variance spatially), the above formula becomes

$$\sigma_n^2 = [\alpha^2 + (1-\alpha)^2]\sigma^2 \tag{5}$$

With $\alpha \in [0, 1]$, we have $\sigma_n^2 \leq \sigma^2$. This means that the noise level will be reduced using the above single source blending method. The worst case is that $\sigma_n^2 = \sigma^2/2$ when $\alpha = 0.5$.

To compensate for this undesired effect, we propose a new way of inserting synthetic nodule by using separate blending for object and noise, so called 'dual source blending' in computer graphics [15]. In this scheme, the nodule object and the noise part are treated as two separate source images, and have different but dependent blending factors. This new dual source blending for lesion insertion can be described as

$$I = \alpha \bar{I}_o + \acute{\alpha} N_o + (1-\alpha) I_b \tag{6}$$

where α the original source blending factor, $\acute{\alpha}$ the new source blending factor introduced specific for noise part. This formula can be extended as

$$I = \bar{I} + n; \quad with \quad \bar{I} = \alpha \bar{I}_o + (1-\alpha)\bar{I}_b, \quad n = \acute{\alpha} N_o + (1-\alpha)N_b \tag{7}$$

with $\bar{I}$ part being same as before, but the combined noise part being changed, compared to formula (3). By assuming $\sigma_o = \sigma_b = \sigma$, the mean and variance of the blended noise are

$$E(n) = 0; \quad \sigma_n^2 = [\acute{\alpha}^2 + (1-\alpha)^2]\sigma^2 \tag{8}$$

To attain same noise levels across core part, volume average layer, and background, we need $\sigma_n^2 = \sigma^2$, i.e., $\acute{\alpha}^2 + (1-\alpha)^2 = 1$. We can set

$$\acute{\alpha} = \sqrt{1 - (1-\alpha)^2} \tag{9}$$

By using dual source blending with blending factors satisfying formula (9), we can maintain the noise level before and after the insertion, under the assumption $\sigma_o = \sigma_b = \sigma$.

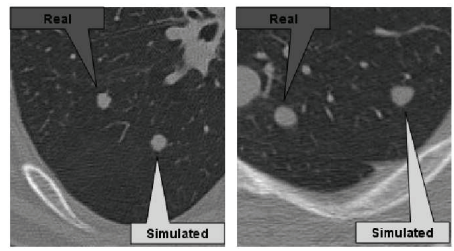

Fig. 3. Illustration of nodule simulation result.

This object insertion method can be easily applied to nodule 'cut and paste' procedure in which a real nodule is 'cut' from its original position, and 'paste' into desired positions. This 'cut' step is actually a segmentation processing; and the 'paste' step is an object insertion procedure. The proposed dual source α blending technique is very suitable for 'pasting' nodules. This 'cut and paste' technique can create 'new' nodules, but is relatively restricted compared to the synthetic model presented in this work.

3 Model Validation

The synthetic nodules simulated from this model were evaluated qualitatively and quantitatively with three studies. First, an expert radiologist carefully reviewed a randomly mixed set of 200 nodules (100 real + 100 synthetic) and provided, for each nodule, a 1 – 10 scale visual rating (1 = not real, 10 = definitely real). Second, the radiologist then rated another random mixed set of 20 nodule cases (10 real + 10 synthetic, with 2 – 10 nodules in each case) on a case by case basis. The ratings were compared between the simulated nodule group and real nodule group. Third, the correlation coefficients of the density attenuation profiles for 20 real nodules and 20 similar sized synthetic nodules were calculated to provide a quantitative measurement of the similarities.

4 Applications for CAD evaluation

A commercial CAD system for automatic lung nodule detection and volume measurement was tested using computer-simulated nodules of various sizes and different contexts (isolated and juxta-vascular) inserted into helical CT exams with different dosages. Two normal CT chest cases (1 low dose = $20mAs$ / 1 regular dose = $120mAs$; both $1.25mm$ collimation) were used as bases for simulation. For each case, two groups (isolated and juxta-vascular) of nodules

with a certain diameter and random shape were inserted. Each group included 50 nodules. Different nodule diameters $(4, 5, 6, 8, 10mm)$ were used. The CAD detection and volume measurement results were scored against the truth.

5 Results

In the model validation studies, 89/100 real nodules and 86/100 synthetic nodules were rated highly realistic (ratings ≥ 7) in the first study, as were 9/10 real cases and 8/10 synthetic cases in the second study, showing no significant statistical difference (Fisher exact test, $p \geq 0.674$). The correlation coefficients of attenuation profiles between simulated and real nodules showed a mean of 0.95 and standard deviation of 0.03.

With regard to CAD evaluation, the CAD detection rates were all 100% except one sub-group ($4mm$ low dose, 98%). The volume measurement errors were similar for different size groups ($6-10mm$: mean $< 2.0\%$, std. $< 2.3\%$; $4-5mm$: mean $\leq 3\%$, std. $< 5\%$). For simulated juxta-vascular nodules, the detection rate gradually deteriorated as nodule size decreased ($6-10mm$: $96+\%$; $5mm$: $86+\%$; and $4mm$: $73+\%$), as did the volume measurement errors ($6-10mm$: mean $< 4.2\%$, std. $< 10\%$; $4-5mm$: mean $< 6.8\%$, std. $< 14\%$). Overall, the CAD performance (detection or volume measurement) was not significantly affected by the different dosages.

6 Discussion

In the literature, the shape of nodules (lesions) was usually represented by simple shapes; the density distribution and attenuation profiles have not been thoroughly investigated; and how to merge the simulated nodule with the background has not been properly solved, especially the noise synthesis.

In this work, by applying randomly generated high dimensional deformations on spheres, we can create very realistic nodule shapes; dissecting nodules layer by layer using distance transform to investigate density distribution and attenuation profiles forms a solid base for simulating the density and the volume average layer; the newly formulated α blending framework for lesion insertion gives a well-understood description of the merging between nodule and background for each pixel. Additionally, the newly designed dual source α blending technique for lesion insertion is able to maintain the noise level across the lesion, the volume average layer, and the background, thus, makes the inserted nodule look more realistic. The Validation demonstrates a high level of similarity between the synthetic nodules and real nodules.

Using the proposed technique, it is possible to conduct a flexible performance evaluation of a CAD system on nodules with different sizes, contexts, shapes, densities, in CT images with different dosages.

The techniques presented in this work, including shape simulation using randomly deformed sphere, object density analysis using distance transform, object

insertion based on dual source α blending, can be easily extended for simulating other lesions, such as colon polyps, mass or calcs in digital mammography/tomosynthesis.

Although the deformed nodule shapes presented in this paper are very realistic, they only represent a small fraction of the possible shapes of real nodules, for example, modeling of highly spiculated nodules, partly solid nodules are not discussed. The main target of this work is to simulate nodules that are most suitable for early detection and accurate estimation of growth – small, somewhat round, solid nodules probably occur most often for early stage pulmonary nodules.

7 Conclusions

We proposed a new simulation model to insert synthetic lung nodules, with shapes and density statistics similar to real nodules, into normal CT chest exams. Nodule shapes were modeled using spheres with added random non-linear deformations. Nodule density and attenuation profiles were analyzed on real nodule samples. The volume average layers were simulated using a dual source α blending between synthesized nodule and real CT background. The synthetic nodules simulated from this model were evaluated qualitatively and quantitatively. These Validation studies demonstrated a high level of similarity between the synthetic nodules and real nodules.

References

1. Giger, M.L., Bae, K.T., MacMahon, H.: Computerized detection of pulmonary nodules in computed tomography images. Investigate. Radiol. **29** (1994) 459–465
2. Armato, S.G., Giger, M.L., Moran, C.J., Blackburn, J.T., Doi, K., MacMahon, H.: Computerized detection of pulmonary nodules on CT scans. Radiographics **19** (1999) 1303–1311
3. Kostis, W.J., Reeves, A.P., Yankelevitz, D.F., Henschke, C.I.: Three-dimensional segmentation and growth rate estimation of small pulmonary nodules in helical CT images. IEEE Transactions on Medical Imaging **22** (2003) 1259–1273
4. Paik, D.S., Beaulieu, C.F., Rubin, G.D., Acar, B., Jeffrey, R.B., Jr., Yee, J., Dey, J., Napel, S.: Surface normal overlap: a computer-aided detection algorithm with application to colonic polyps and lung nodules in helical CT. IEEE Transactions on Medical Imaging **23** (2004) 661–675
5. Zhang, X., McLennan, G., Hoffman, E.A., Sonka, M.: Automated detection of small-size pulmonary nodules based on helical CT images. In: LNCS 3565: Proc. Information Processing in Medical Imaging (IPMI) 2005. (2005) 664–676
6. Mendoca, P.R.S., Bhotika, R., Sirohey, S.A., Turner, W.D., Miller, J.V., Avila, R.S.: Model-based analysis of local shape for lesion detection in CT scans. In: LNCS 3749: Proc. Medical Image Computing and Computer-Assisted Intervention (MICCAI) 2005. (2005) 688–695
7. Zhang, X., Stockel, J., Wolf, M., Cathier, P.: A new method for spherical object detection and its application to computer aided detection of pulmonary nodules in CT images. In: LNCS 4791: Proc. Medical Image Computing and Computer-Assisted Intervention (MICCAI) 2007. (2007) 842–849

8. Armato, S.G., McLennan, G., McNitt-Gray, M.F., Meyer, C.R., Yankelevitz, D., Aberle, D.R., Henschke, C.I., Hoffman, E.A., Kazerooni, E.A., MacMahon, H., Reeves, A.P., Croft, B.Y., Clarke, L.P.: Lung image database consortium: Developing a resource for the medical imaging research community. Radiology **232** (2004) 739–748
9. Raffy, P., Fetita, C., Reigelman, C., Preteux, F., Wood, S., Grenier, P.: Evaluation of computer-aided detection (CAD) performance using mathematically simulated lung nodules. In: Proc. Computer Assisted Radiology and Surgery 2004. (2004) 935–940
10. Zhang, X., Olcott, E., Raffy, P., Yu, N., Chui, H.: Simulating solid lung nodules in MDCT images for CAD evaluation: modeling, validation, and applications. In: Proc. SPIE Medical Imaging 2007. Volume 6514. (2007) 0Z01–0Z08
11. Rexilius, J., Hahn, H.K., Schlter, M., Bourquain, H., Peitgen, H.O.: Evaluation of accuracy in MS lesion volumetry using realistic lesion phantoms. Academic Radiology **12** (2005) 17–24
12. Bookstein, F.L.: Principal warps: thin-plate splines and the decomposition of deformations. IEEE Transactions on Pattern Anal. and Mach. Intell. **11** (1989) 567–585
13. Danielsson, P.E.: Euclidean distance mapping. Computer Graphics and Image Processing **14** (1980) 227–248
14. Razifar, P., Sandstrm, M., Schnieder, H., Lngstrm, B., Maripuu, E., Bengtsson, E., Bergstrm, M.: Noise correlation in PET, CT, SPECT and PET/CT data evaluated using autocorrelation function: a phantom study on data, reconstructed using FBP and OSEM. BMC Med Imaging **5** (2005) 5
15. Angel, E.: Interactive computer graphics: a top-down approach using OpenGL. Addison-Wesley (2003)